

STRUCTURE AND PITTING CORROSION OF Ti-6Al-4V ALLOY AND Ti-6Al-4V WELDS

NIKOLAY VASILEV FERDINANDOV, DANAIL DIMITROV GOSPODINOV,
MARIANA DIMITROVA ILIEVA, ROSSEN HRISTOV RADEV

University of Ruse, 8 Studentska str., Ruse, Bulgaria, mdilieva@uni-ruse.bg

The structure of Ti-6Al-4V alloy and Ti-6Al-4V weldments was examined. The welds were produced by hollow cathode arc discharge in vacuum using tantalum cathodes and different welding parameters. The corrosion behaviour of Ti-6Al-4V alloy and Ti-6Al-4V welds in solution containing Br⁻ was evaluated quantitatively using potentiodynamic polarization tests. The corrosion behaviour of the base metal and welds was compared. Open circuit potential, pitting potential, corrosion current densities and corrosion rates were determined. The influence of the structure and its change during welding on corrosion behaviour is discussed in the present paper.

Keywords: Titanium Alloy, Pitting Corrosion, Welded Joints.

INTRODUCTION

Titanium and titanium alloys are recognized as one of materials with extremely high corrosion resistance but in some specific conditions pitting corrosion of titanium can occur (Petit *et al.*, 1980; Heikal and Awad, 2011; Huo and Meng, 1990). In most environments the welds of titanium and titanium alloys possess the same corrosion resistance as the base metal. Nevertheless, when titanium welds are exposed to marginal or active conditions they can be subjected to accelerated corrosion attacks compared to base metal (Davis, 2006).

Welding of Ti and titanium alloys changes their structure. It is well known that titanium is a highly reactive metal with a standard electrode potential of -1,63 V, and its corrosion resistance is only due to the formation of TiO₂ passive film. The integrity of this passive film is governed by its structure that depends on the underlying metal structure. For instance, coarse metal structure is a condition for formation of less dense oxide layer and thus for facilitation of corrosion processes (Song *et al.*, 2009). The passive film can be destroyed by halide ions as they cause its electrochemical dissolution and open path for aggressive environments through it towards the bare metal surface. Electrochemical dissolution of the oxide layer is not observed only in presence of F⁻, Br⁻, Cl⁻ and I⁻ lead to breakdown of the passive film and Br⁻ are the most effective in this action (Basame and White, 2000). A number of researchers have reported that Ti and its alloys undergo pitting corrosion after polarization in environments containing bromine ions (Garfias-Mesias, 1998; Basame and White, 2000; Dugdale and Cotton, 1964; Beck, 1967; Beck, 1973; Shibata and Zhu, 1995).

The aim of the present work is to examine the corrosion behaviour of Ti-6Al-4V and its welds in an aggressive medium containing bromine ions and to find out relationship between the provoked by welding structural changes and corrosion resistance of the welds.

EXPERIMENTAL PROCEDURE

The material used in this study was 2 mm thick sheet of Ti6Al4V alloy. The specimens were prepared of as-delivered Ti-6Al-4V and of Ti-6Al-4V welded by vacuum arc welding with hollow cathode without filler material and without groove.

The chemical composition of the alloy was obtained by XRF and was as follows: 4.27% V, 6.1% Al, 89.57% Ti. Table 1 shows the welding parameters. The welding was carried out in a device for vacuum arc welding (Gospodinov *et al.*, 2018). After welding, specimens were cut from weldments (Figure 1a) in order to establish their mechanical properties at tensile test.

Table 1. Welding modes

No	Specimen	Current I, A	Welding speed V, m/s	Tantalum foil cathode shape and dimensions, mm	Gas quantity Q, l/h
1	W1	100	4.2	cylindrical Ø4	2.3-2.4
2	W2	115	4.2	cylindrical Ø4	2.3-2.4
3	W3	130	5.5	cylindrical Ø4	2.3-2.4
4	W4	115	5.5	elliptical 5.6 x 2	2.3-2.4
5	W5	130	6.5	elliptical 5.6 x 2	2.3-2.4

After tensile testing (results not presented here) specimens from near the fractured surfaces were cut parallel to welding direction (along the line 1 - Figure 1b) in order to examine welds microstructure and corrosion behaviour. A cross sections normal to welding direction were cut for macrostructure and microstructure examination of weldments. For macrostructural and microstructural analyses specimens were cold-mounted in epoxy resin and prepared by grinding and mechanical polishing, followed by final polishing with Al₂O₃ suspension. Then specimens were etched with a mixture of 15 ml HNO₃, 15 ml HF and 75 ml H₂O for observation of macrostructure and with a mixture of 30 ml C₃H₆O₃, 10 ml HF and 10 ml HNO₃ for microstructural analysis.



Figure 1: a) specimens for tensile testing; b) fractured specimen

The samples for corrosion testing were cold-mounted in epoxy resin, grinded and mechanically polished, cleaned with deionized water and acetone. The analysed surface areas varied between 0.18 cm² and 0.21 cm² as the thicknesses of different welds were different. Potentiodynamic polarisation tests were carried out at room temperature in 1 M KBr aqueous solution open to air. A standard three-electrode cell was used with a saturated calomel electrode (SCE), a Pt counter electrode and the studied sample as a working electrode. All potentials were calculated versus standard hydrogen electrode (SHE). Before polarisation, all specimens were allowed to stabilise for a period of 120 minutes. The scan rate was 1 mV/s. The polarisation potentials changed from -450 mV/SHE to +2200 mV/SHE. Potentiostat RADELKIS OH-405 was used. Using Tafel extrapolation corrosion current densities i_{cor} and corrosion potentials E_{cor} were determined. Pitting potentials E_{pit} were determined from polarisation curves as the points at which a sharp increase in anodic current density was observed. Corrosion rates CR were calculated according to ASTM G102 – 89 (2015). As the fracture of all

specimens was brittle (Figure 1b) it was assumed the tensile testing did not influence the structure and corrosion behaviour of tested specimens.

RESULTS AND DISCUSSION

Structure of Tested Specimens

Figure 2 represents a cross section of one of the Ti-6Al-4V weldments. The remaining specimens had the same macrostructure and are not shown here. The fusion zone (FZ) was composed of coarse ($2\div 3$ mm) grains, elongated towards fusion line. The transition from FZ to heat-affected zone (HAZ) was characterised by inhomogeneous in shape and dimensions grains. Within HAZ grain size decreased towards base metal (BM). The boundary between HAZ and BM was abruptly outlined.



Figure 2. Macrosection of a weldment: 1 – Base metal (BM); 2 – Boundary “Base metal/Heat-affected zone” (BM/HAZ); 3 – Heat-affected zone (HAZ); 4 – Boundary “Heat-affected zone/Fusion zone” (HAZ/FZ); 5 – Fusion zone (FZ)

Figure 3a shows the microstructure of the base metal. The structure of as-received Ti-6Al-4V consisted of two phases: α phase appeared white and intergranular β phase - black. The α -grains were elongated along the rolling direction of the metal sheet that was normal to welding direction. The same microstructure was reported by (Romero *et al.*, 2015). At lower magnification this fine two-phase structure appeared dark – Figure 3b. Figure 3b represents the microstructure at the boundary between the BM and the HAZ. The transition from BM to HAZ showed abrupt changes in microstructural features: grain shape changed from elongated to equiaxed and grain size increased. This fact indicated occurrence of recrystallization and phase transformations in the heat-affected zone implying that the temperature at HAZ was above β transus temperature of the alloy. Within HAZ a gradual increase in grain size was observed: larger grains were formed towards FZ. Near the boundary BM/HAZ the structure of HAZ consisted of comparatively fine, equiaxed recrystallized primary α grains (white) and acicular $\alpha+\beta$ colonies (dark). In the direction of FZ the temperature of HAZ increased gradually during welding and thus phase transformation processes coarsened the microstructure in the same manner - Figure 3c. Meanwhile, the increased temperatures in HAZ towards FZ changed the phase composition: the amount of primary α grains decreased but that of acicular $\alpha+\beta$ colonies increased and colonies of acicular $\alpha'+\beta$ were formed (Figure 3c). A similar microstructure was observed by (Akman *et al.*, 2009; Romero *et al.*, 2015) and it is characteristic for quenching form temperatures below the β transus temperature.

Figure 3d represents the microstructure at the HAZ/FZ boundary and Figure 3e – at the FZ normal to welding direction. The transition from HAZ to FZ was characterised by a mixture of equiaxed and elongated colonies of acicular $\alpha'+\beta$; this microstructure was caused by partial melting. At the FZ acicular $\alpha'+\beta$ colonies of different shape and dimensions were observed together with allotriomorphic α at prior β -grains boundaries. This microstructure implied that the cooling rate at the fusion zone was insufficient for

quenching. The same microstructure at FZ was observed at the tested for corrosion resistance surfaces - Figure 3f, i.e. grain size and shape along the weld and normal to it were identical.

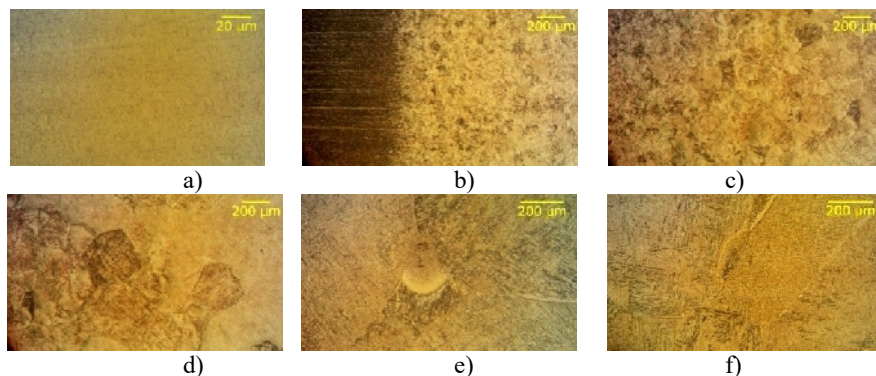


Figure 3. Microstructures of a weldment: a) as-delivered Ti-6Al-4V (position 1 in Figure 2); b) boundary BM/HAZ (position 2 in Figure 2); c) HAZ (position 3 in Figure 2); d) boundary HAZ/FZ (position 4 in Figure 2); e) FZ (position 5 in Figure 2); f) FZ along the weld

Polarisation Behaviour of Ti-6Al-4V and Welds in 1M KBr Aqueous Solution

The voltammetric behaviour of as-delivered Ti-6Al-4V and tested welds is presented in Figure 4. Before anodic polarization all specimens were held in the solution for 120 min. in order to stabilise to OCP. Table 2 summarises the OCPs and the corrosion parameters obtained from polarization curves. OCPs of the welds were lower than that of the BM and this suggested the welds were more prone to corrosion than the BM.

Potentiodynamic polarization curves of Ti-6Al-4V and all welds were similar in shape. The similarity between curves at their cathodic parts indicated that the cathodic reactions on all tested surfaces were alike. As the used medium was neutral, the cathodic reaction was oxygen reduction leading to OH^- formation.

A cathodic current can result in a reduction of the protective oxide layer, thus activating the metal surface (Riskin, 2008). As the corrosion stability of titanium and its alloys is totally dictated by the protective properties of the passive layer, highly reducing potentials can have deteriorating influence on layer's integrity and corrosion resistance. This phenomenon was observed in our experiments and was demonstrated by the differences in OCPs and E_{cor} (Table 2); similar results were reported by (Heakal and Awad, 2011). Moreover, the deteriorating influence of initial cathodic potential in combination with that of Br^- on protective properties of the passive layer led to absence of passive regions at the anodic parts of polarization curves; at anodic parts of all polarization curves, at potentials below 700-800 mV, slow anodic dissolution was observed. The measured anodic current densities of welds were higher than that of the BM and this fact indicated that less stable passive film was formed on welds' surfaces.

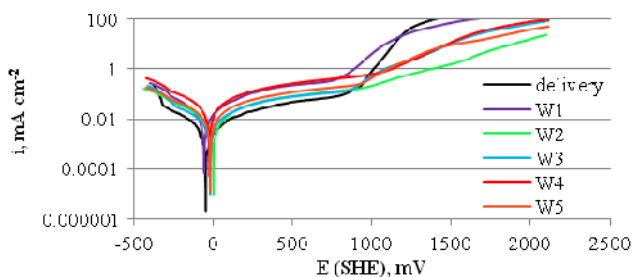


Figure 4. Potentiodynamic polarization curves of Ti-6Al-4V and welds in 1M KBr

Table 2. Electrochemical corrosion parameters of Ti-6Al-4V and weldments

Specimen	OCP, mV	E_{cor} , mV	E_{pit} , mV	i_{cor} , $\mu\text{A cm}^{-2}$	CR, mm/y
As-delivered	115	-44	800	3.6	0.031
W1	25	-58	730	12.6	0.110
W2	75	3	900	9.6	0.083
W3	65	-19	800	4.5	0.039
W4	55	-22	930	23.4	0.203
W5	55	-18	900	9.8	0.085

As the potential increased in positive direction, current densities increased sharply at E_{pit} . Deep wide pits were observed on tested surfaces after polarization - Figure 5. During polarization above E_{pit} a yellow-orange solution was observed directly above the tested surfaces. That colour is characteristic for TiBr_4 and TiOBr_2 . After polarization white precipitates, consistent with TiO_2 and TiO^{2+} , were observed in solution. A similarly coloured solutions and precipitates were observed by (Beck, 1973). These corrosion products and the pitted surfaces of specimens clearly indicated that the sharp rise in current densities was due to pitting corrosion and not only to oxygen evolution. They also indicated that the pitting corrosion mechanism of Ti-6Al-4V and its welds was the proposed by Beck model (Beck, 1973) of salt film formation and its hydrolysis near the metal surface.



Figure 5. Tested in 1M KBr surface of specimen W2 after polarization

The lowest i_{cor} and CR were calculated for as-delivered Ti-6Al-4V (Table 2). This information combined with the highest OCP and lowest anodic current densities below E_{pit} of BM led to conclusion that the welds were with lower corrosion resistance than the BM. The worsen corrosion behaviour of welds was attributed to their coarsened and transformed structure. The oxide film on self-passivating metals generates at grain boundaries. The BM was with finer structure than welded metal thus allowing a denser passive layer to be formed on its surface and to be kept relatively stable.

CONCLUSIONS

The presented experimental results allow the following conclusions to be made:

1) Vacuum arc welding with hollow cathode without filler material and without groove leads to formation of classical welded structures of Ti-6Al-4V.

2) The coarsened structure at the fusion zone of Ti-6Al-4V welds after vacuum arc welding with hollow cathode without filler material and without groove can increase the corrosion rate up to one order.

3) Titanium alloy Ti-6Al-4V and its welds undergo severe pitting corrosion in 1M KBr aqueous solution. The pitting corrosion mechanism is that, described by Beck.

Acknowledgement

This study represents results from work on project №2018-MTF-01 supported by Science Fund at Ruse University “Angel Kanchev”, Bulgaria.

The study was supported by contract of University of Ruse “Angel Kanchev”, № BG05M2OP001-2.009-0011-C01, "Support for the development of human resources for research and innovation at the University of Ruse “Angel Kanchev”. The project is funded with support from the Operational Program “Science and Education for Smart Growth 2014 - 2020” financed by the European Social Fund of the European Union.

REFERENCES

- Акман, Е. *et al.* (2009), “Laser welding of Ti6Al4V titanium alloys”, *Journal of Materials Processing Technology*, 209(8), 3705-3713, <https://doi.org/10.1016/j.jmatprotec.2008.08.026>.
- Basame, S.B. and White, H.S. (2000), “Pitting Corrosion of Titanium - The Relationship Between Pitting Potential and Competitive Anion Adsorption at the Oxide Film/Electrolyte Interface”, *Journal of The Electrochemical Society*, 147(4), 1376-1381, <https://doi.org/10.1149/1.1393364>.
- Beck, T.R. (1967), “Stress corrosion cracking of titanium Alloys: I. Ti:8-1-1 alloy in aqueous solutions”, *J. Electrochem. Soc.*, 114(6), 551-556, <https://doi.org/10.1149/1.2426647>.
- Beck, T.R. (1973), “Pitting of Titanium: I. Titanium-Foil Experiments”, *J. Electrochem. Soc.*, 120(10), 1310-1316, <https://doi.org/10.1149/1.2403253>.
- Beck, T.R. (1973), “Pitting of Titanium: II. One-Dimensional Pit Experiments”, *J. Electrochem. Soc.*, 120(10), 1317-1324, <https://doi.org/10.1149/1.2403254>.
- Davis, J.R. (2006), *Corrosion of Weldments*, ASM International.
- Dugdale, I. and Cotton, J.B. (1964), “The anodic polarization of titanium in halide solutions”, *Corrosion Science*, 4 (1-4), 397-411, [https://doi.org/10.1016/0010-938X\(64\)90041-1](https://doi.org/10.1016/0010-938X(64)90041-1).
- Garfias-Mesias, L. *et al.* (1998), “Determination of precursor sites for pitting corrosion of polycrystalline titanium by using different techniques”, *J. Electrochem. Soc.*, 145(6), 2005-2010, <https://doi.org/10.1149/1.1838590>.
- Gospodinov, D.D. *et al.* (2018), “Welding of Grade 1 titanium by hollow arc discharge in vacuum”, *International Scientific Conference Industry 4.0*, Varna, Bulgaria, 39-41.
- Heakal, F. and Awad, Kh.A. (2011), “Electrochemical Corrosion and Passivation Behavior of Titanium and Its Ti-6Al-4V Alloy in Low and Highly Concentrated HBr Solutions”, *Int. J. Electrochem. Sci.*, 6, 6483 – 6502.
- Huo, Sh. and Meng, X. (1990), “The states of bromide on titanium surface prior to pit initiation”, *Corrosion Science*, 31, 281-286, [https://doi.org/10.1016/0010-938X\(90\)90120-T](https://doi.org/10.1016/0010-938X(90)90120-T).
- Petit, J.A., Kondro, B. and Dabosi, F. (1980), “Ion Beam Analysis Investigation of Pit Nucleation on Titanium in Bromide Media”, *Corrosion*, 36(3), 145-151, <https://doi.org/10.5006/0010-9312-36.3.145>.
- Riskin, J. (2008), *Electrocorrosion and protection of metals*, Elsevier, Oxford.
- Romero, A. *et al.* (2015), “Ti6Al4V titanium alloy welded using concentrated solar energy”, *Journal of Materials Processing Technology*, 223, 284-291, <https://doi.org/10.1016/j.jmatprotec.2015.04.015>.
- Shibata T. and Zhu, Y.-C. (1995), “The effect of film formation conditions on the structure and composition of anodic oxide films on titanium”, *Corrosion Science*, 37(2), 253-270, [https://doi.org/10.1016/0010-938X\(94\)00133-Q](https://doi.org/10.1016/0010-938X(94)00133-Q).
- Song, D. *et al.* (2009), “Corrosion behavior of ultra-fine grained industrial pure Al fabricated by ECAP”, *Transactions of Nonferrous Metals Society of China*, 19(5), 1065-1070, [https://doi.org/10.1016/S1003-6326\(08\)60407-0](https://doi.org/10.1016/S1003-6326(08)60407-0).